Hydrometallurgy 195 (2020) 105388

Contents lists available at ScienceDirect

Hydrometallurgy

journal homepage: www.elsevier.com/locate/hydromet

Leaching kinetics and mechanism of slag produced from smelting-reduction of bauxite for alumina recovery

Fabian Imanasa Azof*, Jafar Safarian

Department of Materials Science and Engineering, Norwegian University of Science and Technology (NTNU), Trondheim, Norway

ARTICLE INFO

Keywords:
Kinetics
Leaching mechanism
Alumina recovery
Calcium aluminate slag
Smelting-reduction bauxite

ABSTRACT

In the present study, we investigate the kinetics and mechanism of the leaching of calcium aluminate slag in Na_2CO_3 solution for alumina recovery. The slag consists of leachable phases, e.g., $12CaO{\cdot}7Al_2O_3$, $CaO{\cdot}Al_2O_3$, $5CaO{\cdot}3Al_2O_3$, and a non-leachable phase that contains Ca-Al-Si-Ti oxides. A series of leaching treatment is done at different temperatures, leaching times, stirring rates, Na_2CO_3 concentrations, and different setups which includes wet-grinding and shaking-digestion reactor. The highest alumina recovery up to 90.5% is obtained after the slag is leached by 10 wt% Na_2CO_3 solution, at low temperatures (30–45 °C) within 90 min. It is shown that the rate of alumina recovery is high at the beginning of leaching and is then slow down due to the calcite layer product nucleation and growth at the surface of slag. The wet-grinding leaching and vigorous stirring increase the possibility of the collision between both particles and the stirrer that breaks the calcite layer, yielding less residue agglomeration and better recovery compared to the slow and mild agitations. A surface observation of the slag using electron microscopy shows that the calcite starts to nucleate at the non-leachable phase as the best deposition site, which has the least mass transfer barrier in the system. The apparent activation energy of the leaching reaction is calculated as 10.8–19.9 kJ/mol, which indicates the reaction is diffusion rate-limited as revealed by the applied kinetic models.

1. Background

Alumina industry is deemed necessary to produce metallurgical grade alumina that has a lower environmental footprint, as the renown Bayer process has been producing a less-utilized residue (red mud) abundantly as nearly as 150 million tons per year (Tsesmelis, 2017). Numerous environmental damage due to mismanaged on red mud disposal has been raised in media, and unfortunately, none of the research projects on red mud valorization have been scaled up to commercial production due to particular challenges. Also, due to a specific use of bauxite that can be treated effectively by the Bayer process, high dependency of alumina industry on high-grade bauxite ores mined only from particular regions, i.e., near-equatorial zone, to get lateritic bauxite is favored.

Exciting results from one of the alternative processes for a sustainable alumina recovery have been reported in the literature (Azof et al., 2017, 2018; Blake et al., 1966; Fursman et al., 1968; Miller and Irgens, 1974; Safarian and Kolbeinsen, 2016a, 2016b; Sellaeg et al., 2017). The process is based on a smelting-reduction of the bauxite with subsequent leaching of the obtained aluminate slag in a sodium carbonate solution. It was invented by Harald Pedersen, which was later called the Pedersen process, in 1927 (Pedersen, 1927). The process is proper for the successful recovery of alumina and iron from the bauxite, while no red mud is produced. A schematic of the Pedersen process can be seen in the supplementary material.

Authors' studies on the leaching characteristics of synthetic CaO-Al_2O_3 slags and a slag produced from the smelting-reduction of commercial low-grade bauxite have been published earlier (Azof et al., 2019, 2020). The kinetics behavior and the mechanisms of the leaching reactions in the Pedersen process are still unclear as the occurring solid-fluid reaction during the leaching is considerably complicated, and there is no significant published work in this area. Therefore, the present work is now focused on the experimental study of the leaching kinetics of calcium aluminate slags. Innovative electron microscopy study on the samples is applied to discover the growth of solid product during leaching. Moreover, different kinetic models are evaluated for the experimental results to determine the process rate-limiting steps and outline the mechanism of leaching.

2. Leaching reactions

Typical leaching reactions of the Pedersen process were stated in the

* Corresponding author.
E-mail address: fabian.i.azof@ntnu.no (F.I. Azof).

https://doi.org/10.1016/j.hydromet.2020.105388
Received 21 December 2019; Received in revised form 15 May 2020
Available online 05 June 2020

literature (Azof et al., 2017; Blake et al., 1966) and are shown in Eqs. (1) and (2). The change of standard Gibbs energy is also presented after each equation, as calculated from a thermochemistry software HSC™. In general, the reactions involve leachable calcium aluminate phases, such as $CaO{\cdot}Al_2O_3$ (denoted as CA), $12CaO{\cdot}7Al_2O_3$ (denoted as $C_{12}A_7$), and $5CaO{\cdot}3Al_2O_3$ (denoted as C_5A_3) phases, Na_2CO_3, and H_2O. Thus, the reactions produce:

(1) $NaAlO_2$ in an aqueous phase, which is an aluminum-rich soluble phase that is later precipitated by carbonation after the leaching process, and.
(2) A leaching residue as the byproduct, which is also referred to as grey mud, and it predominantly consists of $CaCO_3$ and unreacted slag (Vafeias et al., 2018).

$$CaO{\cdot}Al_2O_{3(s)} + Na_2CO_{3(aq)} = NaAlO_{2(aq)} + CaCO_{3(s)} \quad (1)$$

$$(\Delta G^{\circ}_{25°C} = -53.6\ kJ/mol CaO{\cdot}Al_2O_3)12CaO{\cdot}7Al_2O_{3(s)} + 12Na_2CO_{3(aq)} + 5H_2O_{(l)} = 14NaAlO_{2(aq)} + 12CaCO_{3(s)} + 10NaOH_{(aq)} (\Delta G^{\circ}_{25°C} = -745.2\ kJ/mol 12CaO{\cdot}7Al_2O_3) \quad (2)$$

Based on authors' recent study on the morphology and cross-section analysis of the grey mud (Azof et al., 2019), the polymorph of $CaCO_3$ (e.g., calcite, aragonite, vaterite) nucleated and covers the surface of the slag, meanwhile the unreacted slag remains inside of the core. The illustration of the depolymerization of calcium aluminate slag in Na_2CO_3 solution and $CaCO_3$ formation at the surface of slag can be seen in the supplementary material.

3. Solid-fluid kinetics equation for spherical particles

The kinetics equation of solid-fluid reactions in a leaching process can be treated similarly to the solid-gas reaction. The type of heterogeneous reaction to being considered is the reaction of a solid and a liquid that yields solid and liquid products. A spherical reacting particle as one of the most practical models in the kinetics equation, also used in this study to simplify the calculations. In the authors' recent work (Azof et al., 2019), we have managed preliminary works about the kinetics behavior of a calcium-aluminate slag that was leached in a sodium carbonate solution. The data was reasonably in good agreement with Ginstling – Brounshtein's equation (Ginstling and Brounshtein, 1950) and the “ash diffusion” equation in the shrinking core model (Levenspiel, 1999; Yagi and Kunii, 1955). These may indicate that the slag leaching reaction is diffusion rate controlled. In the current study, we plot the kinetics data obtained against the equation that belongs to that of rate controlled and investigate the results of the best model-fit. The list of equations used in the study and its model assumption is added as supplementary material.

4. Experimental methodology

The experiments carried out in this study are elaborated in three different sections, i.e., slag preparation, description of the leaching setups, and techniques used to characterize the samples.

4.1. Slag preparation

The starting material used in this work is a slag that was produced from a smelting-reduction process of low-grade bauxite from our previous work (Azof et al., 2018). The low-grade bauxite was mixed with lime in a mass ratio of CaO/Al_2O_3 equals to 1.0. The ratio was chosen so that the produced slag would have leachable phases in a sodium carbonate solution, as claimed in the literature (Blake et al., 1966). Based on an X-Ray Diffraction (XRD) analysis, the slag consists of $C_{12}A_7$ as the major phase, including CA and C_5A_3, as the minor phases. The chemical composition of the low-grade bauxite and the produced slag were analyzed by X-Ray Fluorescence (XRF), and the results are shown in Table 1.

Table 1
Normalized XRF analysis of the low-grade bauxite and the produced slag.

Materials	Constituents (wt%)					
	Al_2O_3	CaO	SiO_2	TiO_2	Fe_2O_3	MgO
Low-grade bauxite	65.4	4.4	4.1	3.2	22.7	0.2
Slag	46.1	48.1	2.3	1.8	0.9	0.5

Due to a practical reason, we need to use a relatively fine size of slag for the leaching experiment. Therefore, the slag was ground with Retsch™ ring mill for 30 s in 700 rpm. The size distribution of the slag was then measured by using Horiba™ LA-960 in a wet analysis, which was isopropanol based with a refractive index of 1.378.

4.2. Leaching setups and characterization techniques

There are two different leaching setups used in the current work. First, a setup for the leaching kinetics observation. Moreover, the second setup is for the investigation of the leaching mechanism.

4.2.1. Leaching kinetics experimental setup

In the kinetics experiment, 10 g of slag was leached with 200 mL of Na_2CO_3 solution in a borosilicate glass at 30, 45, 60, and 90 °C. No silicon contamination from the glass container was detected on the blank solution. Furthermore, 3 and 10 wt%Na_2CO_3 solvent concentrations were chosen to observe different concentrations effect to the aluminum recovery. The first concentration represents the Pedersen original leaching process (Pedersen, 1927). Whereas, the latter was chosen according to our unpublished preliminary trials.

The ratio of solid to liquid is 5% in mass, and is assumed constant throughout the leaching treatment, as the water evaporation was considered small; less than 10%. The solid and liquid were stirred at 60, 150, and 300 rpm using a magnetic bar stirrer. The leaching time was up to 90 min. Moreover, during the leaching 3 ± 0.3 mL of the solution were taken as a sample in different periods. The samples were filtered by using a Büchner funnel and an ashless grade of quantitative filter paper, which then separated the liquor and the solid (grey mud). Also, for the kinetics experiment in a 3 wt%Na_2CO_3 solution, forty PTFE-balls with a diameter of 6 mm were used to increase the agitation and collision effects.

The chemical compositions of the liquors were analyzed using Inductively Coupled Plasma-High Resolution-Mass Spectroscopy (ICP-HR-MS) Agilent 8800™. On the other hand, the grey mud was qualitatively analyzed using Bruker D8 A25 DaVinci™ XRD machine with CuKα radiation, between 10 and 75° diffraction angle, 0.01° step size, and 2.5° for both primary and secondary soller slit.

Moreover, we used a digestion reactor that can be shaken to elucidate the effect of various agitation mechanisms on the progress of leaching reactions. The digestion reactor is a Polytetrafluoroethylene (PTFE)-base with a capacity of 45 mL and covered with stainless steel as the outer body. It was placed on a tilting plate that can move ± 45° from the horizontal situation, which gives a shaking effect to the solution inside the reactor. The leaching setup using the borosilicate glass and digestion reactor can be seen in the supplementary material.

4.2.2. Leaching mechanism experimental setup

In the current setup, the objective is to study the leaching mechanism and the growth of the solid product (calcium carbonate) that occurs on the slag's surface while it is being exposed to Na_2CO_3 solution. To achieve that, we submerged the polished slag, which was previously cast into a resin, into a 10 wt% Na_2CO_3 solution for short intervals, while a magnetic stirrer stirred the solution at 300 rpm. The

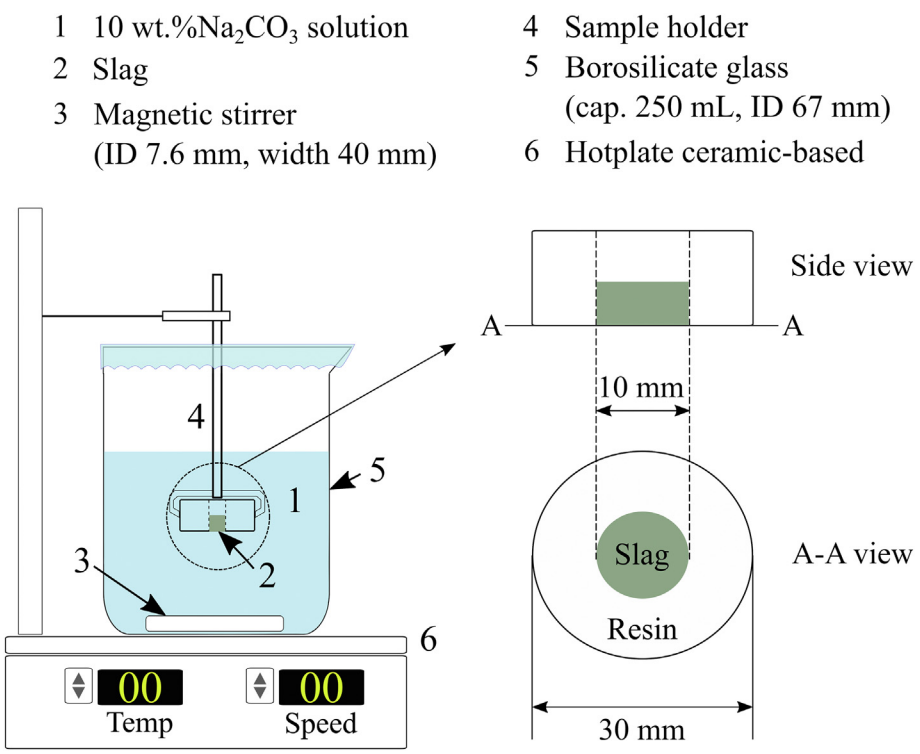

Fig. 1. Leaching mechanism experimental setup.

leaching setup is shown schematically in Fig. 1.

The morphology of the surface of the slag was investigated using Hitachi SU6600™ Scanning Electron Microscope (SEM) after 30 s, 1, 5, 10, and 60 min of the leaching treatment. Furthermore, the elemental mapping and chemical composition of the investigated phases were analyzed by X-Ray element mapping and Energy Dispersive Spectroscopy (EDS) in the SEM.

5. Results and discussion

Results of five different subjects are presented and discussed in the current section; characteristics of the slag, aluminum recovery extent, pH property and thermochemical reactions, leaching kinetics, and characteristics of the leached surface of the slag in different durations.

5.1. Characteristics of the slag

Typical Back-Scattered Electron (BSE) images of the cross-section of the slag at 500× and 1500× magnifications are shown in Fig. 2. Due to the different contrast (light and dark) displayed on the image, at least two distinct phases co-exist and can be identified from the slag. As shown previously in Table 1, the slag has Ca and Al as the dominant elements, and Si and Ti as the minor ones. The light contrast represents a dense phase that may consist of Ca-Al-Si-Ti elements. Whereas, the darker one represents a lighter phase that only may have Ca—Al elements, which is the major phase, the $C_{12}A_7$ phase.

Also, Fig. 3 shows the X-ray mapping of major elements in the dashed-square area of the slag. It shows that the phase with light contrast has more of Al, Si, and Ti than the darker one. This phase is non-leachable in Na_2CO_3 solution (in the applied conditions); therefore, for further notation, we use a non-leachable phase to refer to this phase.

The size distribution of the ground slag is shown in Fig. 4. The size is

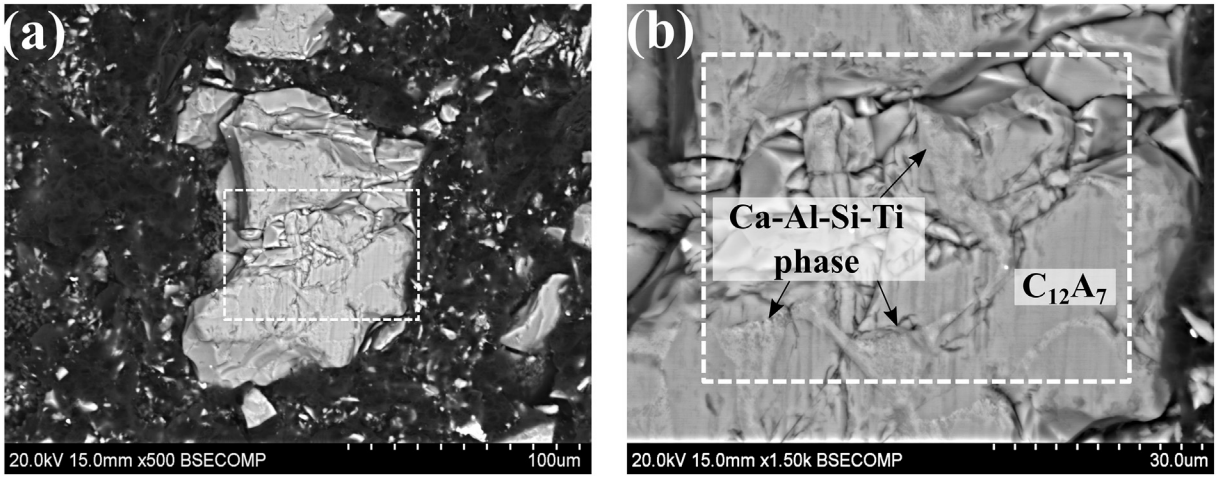

Fig. 2. BSE images of the cross-section of slag at (a) 500× magnification and (b) 1500× magnification.

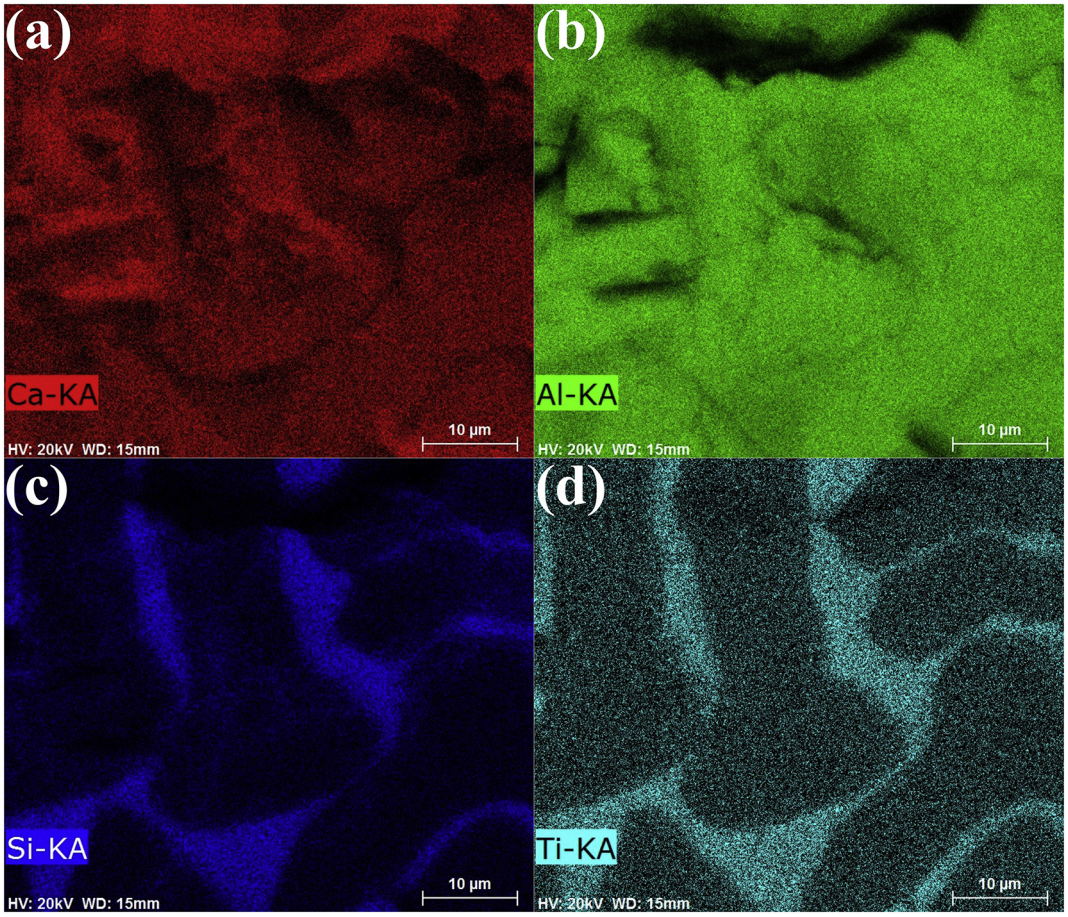

Fig. 3. X-ray mapping elements of the white-dashed square of the slag cross-section in Fig. 2 that shows (a) calcium, (b) aluminum, (c) silicon, and (d) titanium-rich areas.

less than 100 μm, which is considered a fine particle. Based on the size distribution wet analytical results, the value of D_{10}, D_{50}, and D_{90} of the slag are 7.3, 21.2, and 56.5 μm, respectively.

5.2. Aluminum recovery extent

We investigated the effects of different leaching conditions to the aluminum recovery extent, which are temperature, Na_2CO_3 concentration, stirring rate, and particle collision.

5.2.1. The effect of temperature and Na_2CO_3 concentration

Fig. 5 shows the effect of different leaching temperatures, 30 and 45 °C, to the aluminum recovery extent, which uses 10 wt%Na_2CO_3 concentration, at 300 rpm of stirring rate, and in 90 min of leaching time. As seen, the recovery from the slag is considerably high even in the short leaching times, i.e., 15 min, 75% on 30 °C-sample, and 81.8% on 45 °C-sample, on average. The result indicates that the leaching reaction starts immediately as the surface of the slag is contacted with the solution. The recovery increases slowly as the leaching time

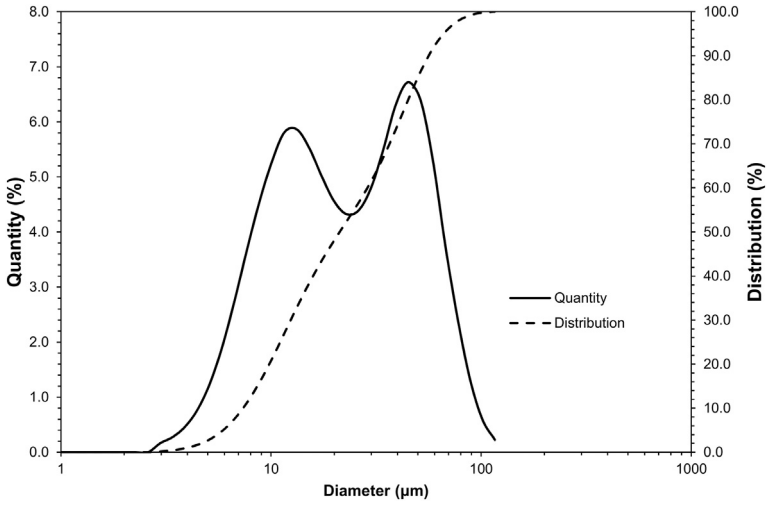

Fig. 4. The size distribution of the slag.

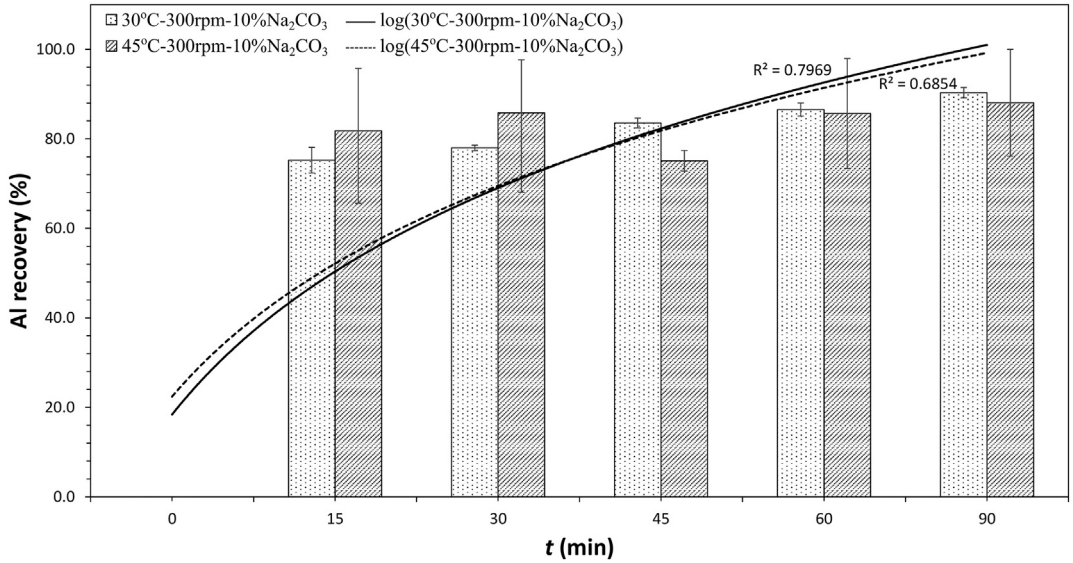

Fig. 5. Aluminum recovery (%) as a function of time (min) at 30 and 45 ˚C of leaching temperature with following conditions: 300 rpm of stirring rate, use of magnetic stirrer, and 10 wt% Na_2CO_3 of the solvent's concentration.

progresses. After 90 min of the treatment, the recovery is 90.3% and 88% for 30 and 45 ˚C, respectively. However, as the deviation bar of 45 ˚C-sample at 90 min is ± 13%, this suggests that it is possible to recover almost all the soluble aluminum from the slag, except the small portion in the minor non-leachable phase. We may conclude that by 10 wt%Na_2CO_3 solution, the recovery increases 8–10% as the temperature rises from 30 to 45 ˚C.

Fig. 6 shows the aluminum recovery (%) as a function of time at 45 and 90 ˚C in leaching trials that 3 wt%Na_2CO_3 was used as the solvent, at 300 rpm of stirring speed, and as an addition to the magnetic bar stirrer, PTFE-balls were also used to strengthen the agitation. The recovery difference is significant between the two temperatures. At 5 min, the recovery is 56.1 and 74.7% for 45 ˚C and 90 ˚C-samples, on average. The recovery increases slowly as the leaching time progresses, which is like what was occurred on the previous leaching conditions using 10 wt %Na_2CO_3. At the same solvent and stirring conditions, the recovery increases 43%, on average, as the leaching temperature rises from 45 to 90 ˚C. Furthermore, as is seen in Fig. 6, the recovery percentage of 45 ˚C-sample from 3 wt%Na_2CO_3 solution is lower compared with that in 10 wt%Na_2CO_3 solution (Fig. 5). At 30 min, the recovery of 45 ˚C-sample is 54.8% in 3 wt%Na_2CO_3 and 85.8% in 10 wt%Na_2CO_3 solution. On average, the recovery increases by 46% as the Na_2CO_3 concentration changes from 3 to 10 wt%Na_2CO_3.

5.2.2. *The effect of stirring speed and particle collision*

The slags were leached on different stirring speeds at 45 ˚C in 10 wt %Na_2CO_3 solution. The order from the strongest to the mildest agitation is 300 rpm, 60 rpm, and 50 shakings per min (spm). The first two experiments were performed on the hotplate ceramic-based, while the latter was performed on the digestion reactor using the tilting plate. Furthermore, Fig. 7 shows that within the same leaching time, the highest recovery is achieved from the most vigorous agitation. On the other hand, the mildest one results in the lowest recovery.

It was documented before in the authors' previous work (Azof et al., 2019) that the grey mud tended to agglomerate when the leaching was performed in a mild agitation. The crystalline bridges induced by calcite crystal growth cause the agglomeration, which leads to a hard cement-like particle. The cross-section observation of the grey mud residue (Azof et al., 2019) also shown that the calcite formation and growth on the slag particles might hinder the contact between Na_2CO_3

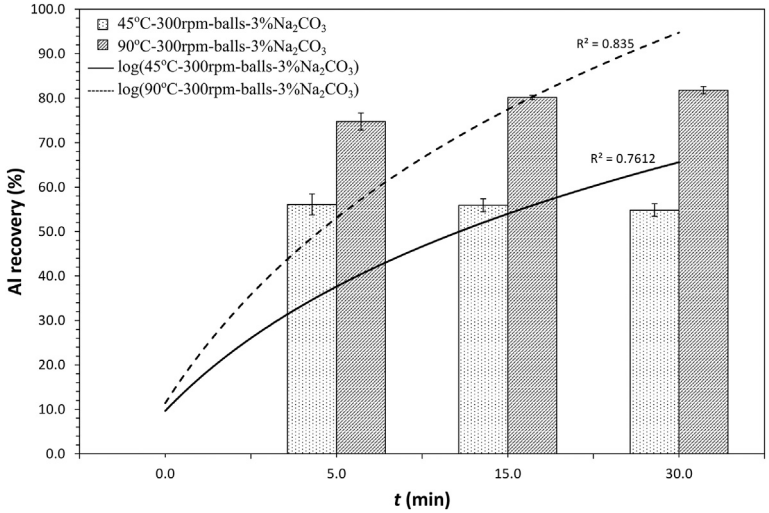

Fig. 6. Aluminum recovery (%) as a function of time (min) at 45 and 90 ˚C of leaching temperature with following conditions: 300 rpm of stirring rate, use of magnetic stirrer, and PTFE-balls, and 3 wt% Na_2CO_3 of the solvent's concentration.

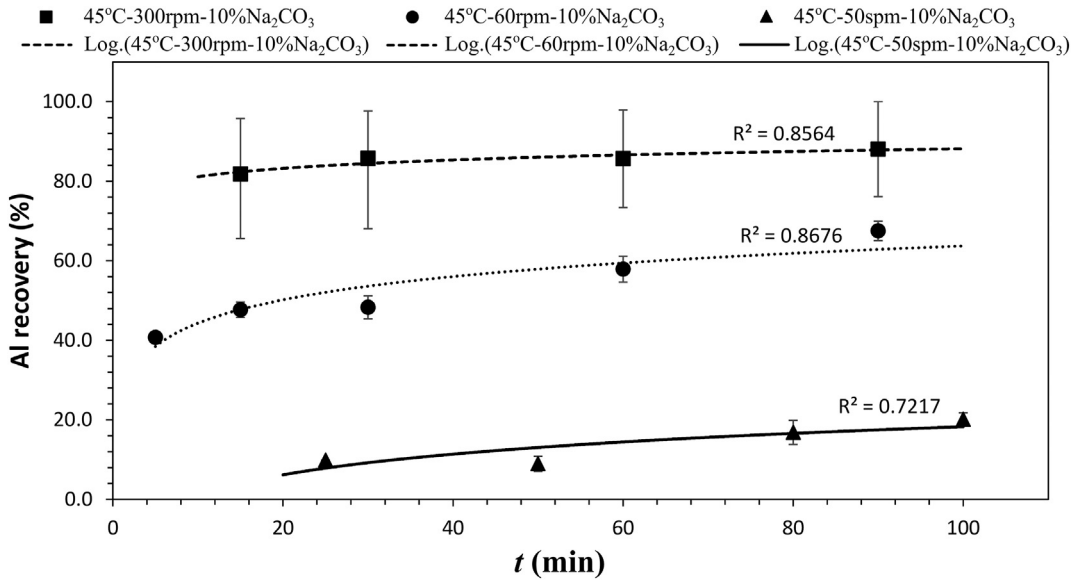

Fig. 7. Aluminum recovery (%) as a function of time (min) at 45 °C of the leaching temperature at different stirring rates in 10 wt%Na_2CO_3 of the solvent concentration.

and the soluble calcium aluminate phases. Therefore, following the result in Fig. 7, it shows that the agitation using a magnetic bar stirrer at a higher rate increases the possibility of the collision between both particles and stirrer that breaks the calcite layer, yielding less grey mud agglomeration, which results in better recovery compared to the slow and mild agitations.

5.3. The pH property and thermochemical reactions during the leaching

The pH and temperature measurements on one of the leaching trials at 45 °C, at 150 rpm, in 10%Na_2CO_3 solutions are shown in Fig. 8. The experiment was intended to elucidate the leaching effects on the pH property of the solution and its thermochemical reactions. The notations in the figure are described in Table 2.

5.4. Residue characteristics and the reacting slag surface

Samples of the solid residue (grey mud) were taken after 5, 15, 30, 45, and 60 min of leaching at 45 °C, 300 rpm of stirring rate, in 3 wt% Na_2CO_3 solution. Fig. 9 shows the normalized XRD patterns obtained from samples, which are compared with the unleached slag. As seen, after 5 min of leaching, the calcite exists in the grey mud as the major phase. Other minor phases in the grey mud are $C_{12}A_7$, C_5A_3, and aragonite (another polymorph of $CaCO_3$). The CA peaks are relatively low and nearly undetected in the grey mud, as it may have already leached.

Another distinct pattern that can be seen from the XRD result is the $C_{12}A_7$ phase, and the intensity of peaks are decreased as the leaching progresses, indicating that the dissolution proceeds, as the calcite nucleates.

The SEM images of the surface of the slag after being exposed in 10 wt%Na_2CO_3 solution at different times are shown in Fig. 10. The instrument setup used for the experiment was schematically shown earlier in Fig. 1. Based on the above results and these SEM observations, the leaching mechanism can be described as follows:

(a) The 30-s images in Fig. 10(a) show that calcite crystals

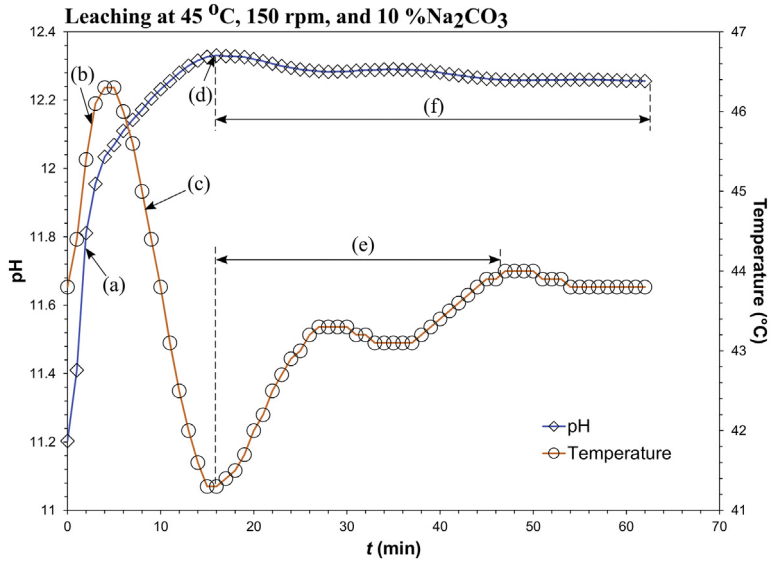

Fig. 8. The pH and temperature (°C) measurement of the leaching solution as a function of time (min). The description of the notations is presented in Table 2.

Table 2
Description of the notations in pH and temperature measurement.

Notation	Description
(a), (b)	Showing an immediate increase in pH and temperature at the beginning (< 5 min). According to the leaching reaction (2), a reaction between one mole of $C_{12}A_7$ and ten moles of Na_2CO_3 produces 10 mol of NaOH, which is a strong alkali compound that increases the pH. On the other hand, an exothermic reaction between aqueous AlO_2^- and Na^+ phase that produces $NaAlO_{2(aq)}$ as in Eq. (3), explains the rise in temperature. $AlO^-_{2(aq)} + Na^+_{(aq)} = NaAlO_{2(aq)}$ (3) ($\Delta H^\circ_{25^\circ C}$ = - 0.9 kJ/mol$NaAlO_2$)
(c)	Indicating the decrease of temperature as the endothermic reaction, which is shown in Eq. (4), starts to occur. In the meantime, the dissolution of the soluble $C_{12}A_7$ phase continues as the pH remains increasing at this period (5–15 min). $Ca^{2+}_{(aq)} + CO^{2-}_{3\,(aq)} = CaCO_{3(s)}$ (4) ($\Delta H^\circ_{25^\circ C}$ = 13.6 kJ/mol$CaCO_3$)
(d)	The highest point of the pH in the reaction is obtained. It occurs after 15 min of leaching. The point also marks the steepest drop of temperature (about 5 °C) and indicates that the leaching reaction (2) may have reached its equilibrium.
(e)	The temperature of the solution increases as the heat supplied by the hotplate rises to target the set point. The hotplate increases the heat of the solution as the temperature was dropped and is lower than its set point.
(f)	Indicating the plateau of the pH as the leaching reaction goes considerably slow. The small changes in the pH are influenced by the correction of the temperature and slow leaching reactions.

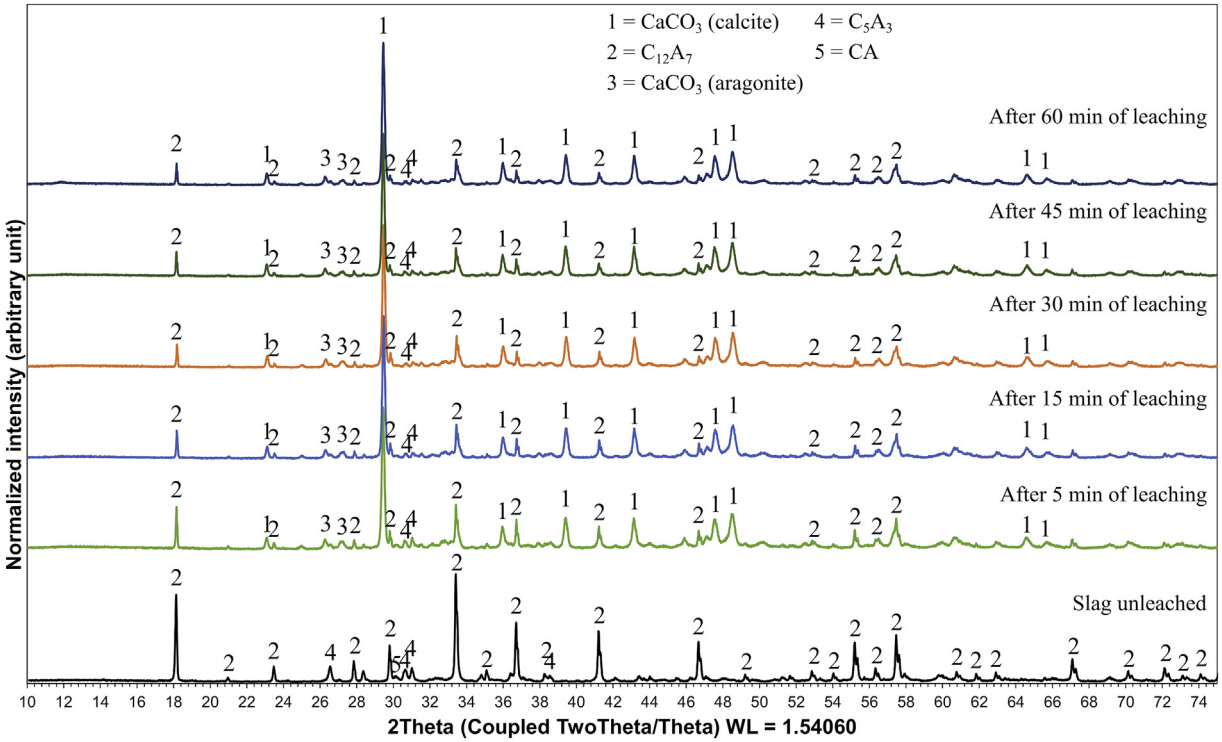

Fig. 9. Normalized XRD patterns of the slag and leached slag within 5, 15, 30, 45, and 60 min at 45 °C, 300 rpm of stirring rate, and 3 wt%Na_2CO_3 of solvent concentration.

(1 ± 0.5 μm) are nucleated at the surface of the non-leachable phase. The non-leachable phase acts as a precursor of the calcite. A topological difference between the surface of $C_{12}A_7$ and the non-leachable phase indicates the depolymerization of the $C_{12}A_7$ phase. Some microcracks on the surface of the $C_{12}A_7$ are also apparent.

(b) Within 1 min leaching, more calcites are nucleated at the surface of the non-leachable phase and in boundaries between resin and slag (see Fig. 10(b)), in which the sites are considerably more stable than $C_{12}A_7$. Meantime, the topological surface between $C_{12}A_7$ and non-leachable phases looks more distinct than before.

(c) As shown in Fig. 10(c), after 3–5 min leaching, the calcite grows up to 100–150% of its previous size. The cracks on the $C_{12}A_7$ surface, which are resulted from the leaching, are seemed to be more apparent. Some locations in the $C_{12}A_7$ phase are probably more susceptible to the dissolution, or dissolution occurs in preferred directions of the $C_{12}A_7$ crystal.

(d) The calcites have covered all the available surfaces of the slag, as shown in Fig. 10(d) after 10 min of leaching due to the precipitation, growth, and accumulation of the calcite crystals in plates parallel to the reacting surface. At this period, the rate of leaching reactions might significantly decrease as the calcite is an inert phase, and the $C_{12}A_7$ phase is not much in direct contact with Na_2CO_3 solution. The calcites growth and networking behavior are similar to the literature observation after Nancollas (Nancollas and Reddy, 1971).

In addition to the surface morphologies described above, a BSE image and EDS spectrum on the surface of slag after 1 min leaching are shown in Fig. 11(a) – (c). The EDS of points 1–4 shows high Ca-Al-Si-Ti-O intensities, which indicates that the observed points are on the non-leachable phases. Meanwhile, the EDS of points 5–8 show that this phase is $C_{12}A_7$, as only Ca-Al-O intensities are noticeable. The composition of the slag based on EDS point analysis is presented in Table 3.

Also, an X-ray mapping of the slag's surface shown in Fig. 11(a) is

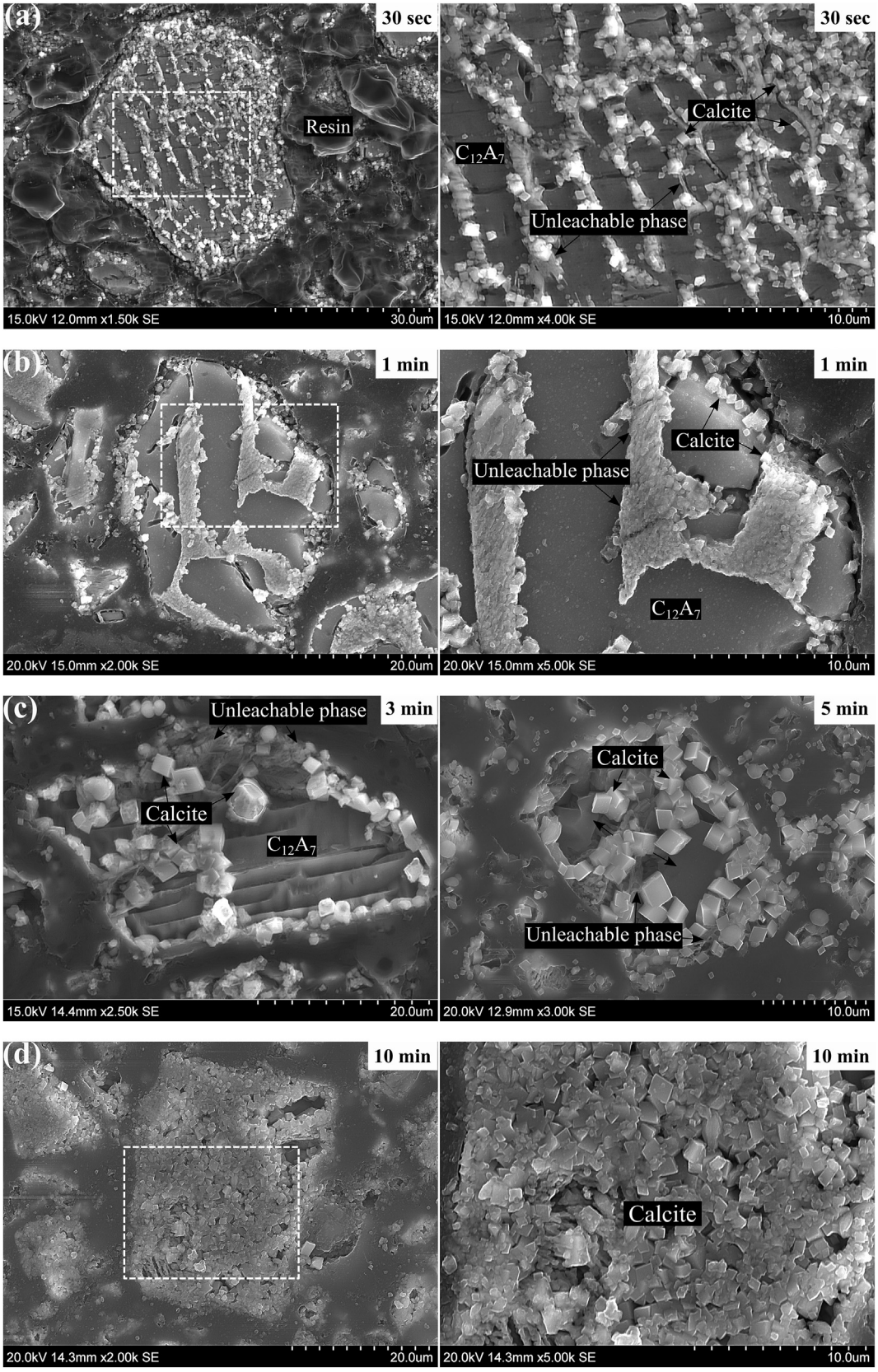

Fig. 10. SEM images of the surface of slag after being exposed to 10 wt%Na_2CO_3 solution for (a) 30 s at 1500× and 4000× magnifications, (b) 1 min at 2000× and 5000× magnifications, (c) 3 and 5 min at 2500× and 3000× magnifications, respectively, and (d) 10 min at 2000× and 5000× magnifications.

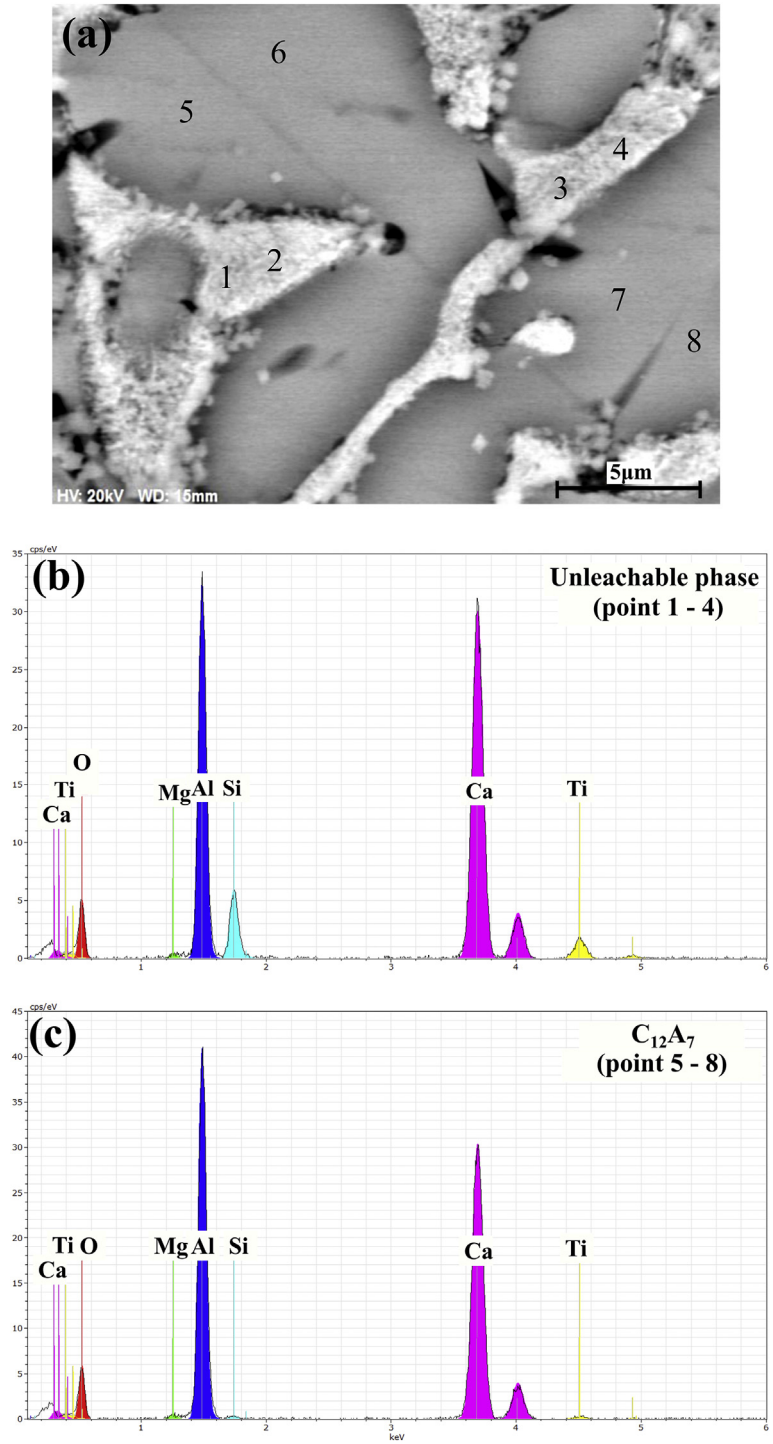

Fig. 11. (a) BSE image of the surface of slag after 1 min of leaching treatment, and the EDS spectrum of (b) non-leachable phase, and (c) the $C_{12}A_7$ phase.

Table 3
Composition of the slag based on EDS point analysis in Fig. 11.

Point	Ca (wt%)	Al (wt%)	Si (wt%)	Ti (wt%)	Mg (wt%)	O (wt%)
1–4	37.4	22.7	3.9	3.0	0.3	32.8
5–8	38.6	30.2	0.3	0.6	0.4	30.1

provided in Fig. 12. As seen, the extent of silicon and titanium concentrations on the non-leachable phase is greater than that of the $C_{12}A_7$ phase. On the other hand, the extent of calcium and aluminum concentrations on the non-leachable phase is less than that of the $C_{12}A_7$, which correlates with the EDS point analysis (Table 3). Furthermore, it was shown previously in Fig. 10 that calcite particles nucleated on the surface of the non-leachable phase shortly after the leaching starts. However, the calcites are hardly recognizable both in EDS point analysis and X-ray mapping results due to thin thickness.

Based on the obtained results, in Fig. 13, we illustrate the mechanism of calcite nucleation and growth on the slag during the leaching of $C_{12}A_7$ in Na_2CO_3 solution from a cross-section view. At the beginning of the leaching, the mass transfer rate is distinctly high. Meantime, calcite crystal starts to nucleate at the non-leachable phase as a proper location and also in a short distance for ions transfer that the

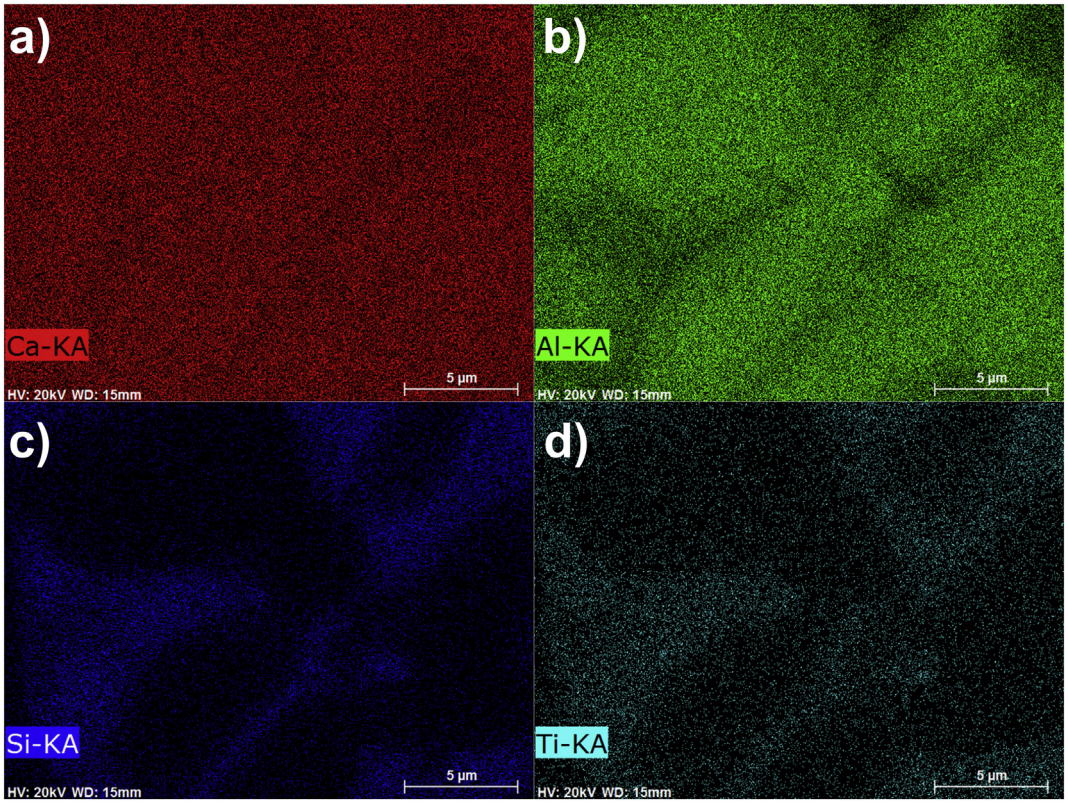

Fig. 12. X-ray mapping element of the surface of slag after 1 min of leaching.

reaction proceeds. Thus, when the calcite grows simultaneously with the leaching of $C_{12}A_7$, the calcite growth occurs in both directions from over the non-leachable phase, in a vertical direction to the slag surface and a parallel direction to the slag surface. The latter growth is accompanied by the coverage of the leachable $C_{12}A_7$ phase, which eventually covers the entire slag surface. Hence, after the growth of the calcite, the leaching reaction is reduced due to less contact between the slag and the solution, and in long reaction times, the mass transfer rate is significantly low. When the surface is mostly covered by the calcite, the diffusion of the reacting aqueous phases (Ca^{2+}, AlO_2^-, Na^+, CO_3^{2-}) through the product calcite layer controls the rate of reaction.

5.5. Leaching kinetics of the reacting slag

5.5.1. Diffusion models

In the current study, it is convenient to denote the yield of aluminum recovery (%) as the fraction of conversion (α). Furthermore, we may plot the integrated form of reaction models, ($F(\alpha)$), against the leaching time from different conditions, as shown in Fig. 14(a) – (c).

In Fig. 14(a) the model of Zhuravlev, Lesokhin, and Templeman (ZLT) and Ginstling – Brounshtein (GB) has a positive correlation and closer interception to the origin, compared with the other models. On the other hand, Fig. 14(b) and (c) show that the model of GB-equation fits better than the other models. These results are in accordance with our previous work, which suggested that GB-equation is one of the most fitted equations for the leaching of the calcium aluminate slag (Azof et al., 2019).

ZLT model calculates the rate based on Jander-equation for spherical particles and considers that the concentration of penetrating species does not remain constant and is proportional to the fraction of the unreacted conversion (1 – α). Meanwhile, GB does not consider the change of penetrating species concentration during the treatment. However, they had been derived by introducing the Fick's first law to the parabolic law's equation and been corrected the oversimplified "three-dimensional" calculation made by Jander (Khawam and Flanagan, 2006; McIlvried and Massoth, 1973).

It is worth noting that the slag particles in the present study do not have a spherical shape and are not uniform in size. The irregular shapes and distributed size made the models less accurate. Also, there is evidence from the results of pH property and thermochemical reactions (shown in Section 5.3) that different mechanisms were occurring during the leaching treatment. Different leaching mechanisms cause the model, which is only significantly based on one controlled reaction, e.g., diffusion, does not properly fit for a complete leaching process.

5.5.2. Process rate

As discussed earlier, different mechanisms are occurring throughout the leaching process. Different mechanisms attributed to different process rate constants. Based on the aluminum recovery extent and pH changes shown earlier in Section 5.2 and 5.3., there are up to three different process steps that may occur in series during the leaching process:

1. The chemical reaction rate-controlling step, which is denoted by k_{chem}, between the leachable phases and Na_2CO_3 solution at the surface of slag.
2. The penetration and diffusion of reactants, which is denoted by $k_{diff.react}$, i.e., Na^+, CO_3^{2-}, H_2O, to the unreacted slag (core) through the calcite layer
3. The outward diffusion of products, which is denoted by $k_{diff.prod}$), i.e., AlO_2^-, OH^-, through the calcite layer to the leachate. The current step may also include the transportation of Ca^{2+} ions from the reaction interface to the proper site, which leads to the deposition of $CaCO_3$.

According to Levenspiel (Levenspiel, 1999), we may account for the simultaneous steps above as an individual resistance occurring in the process because it is not reasonable to consider that one step controls

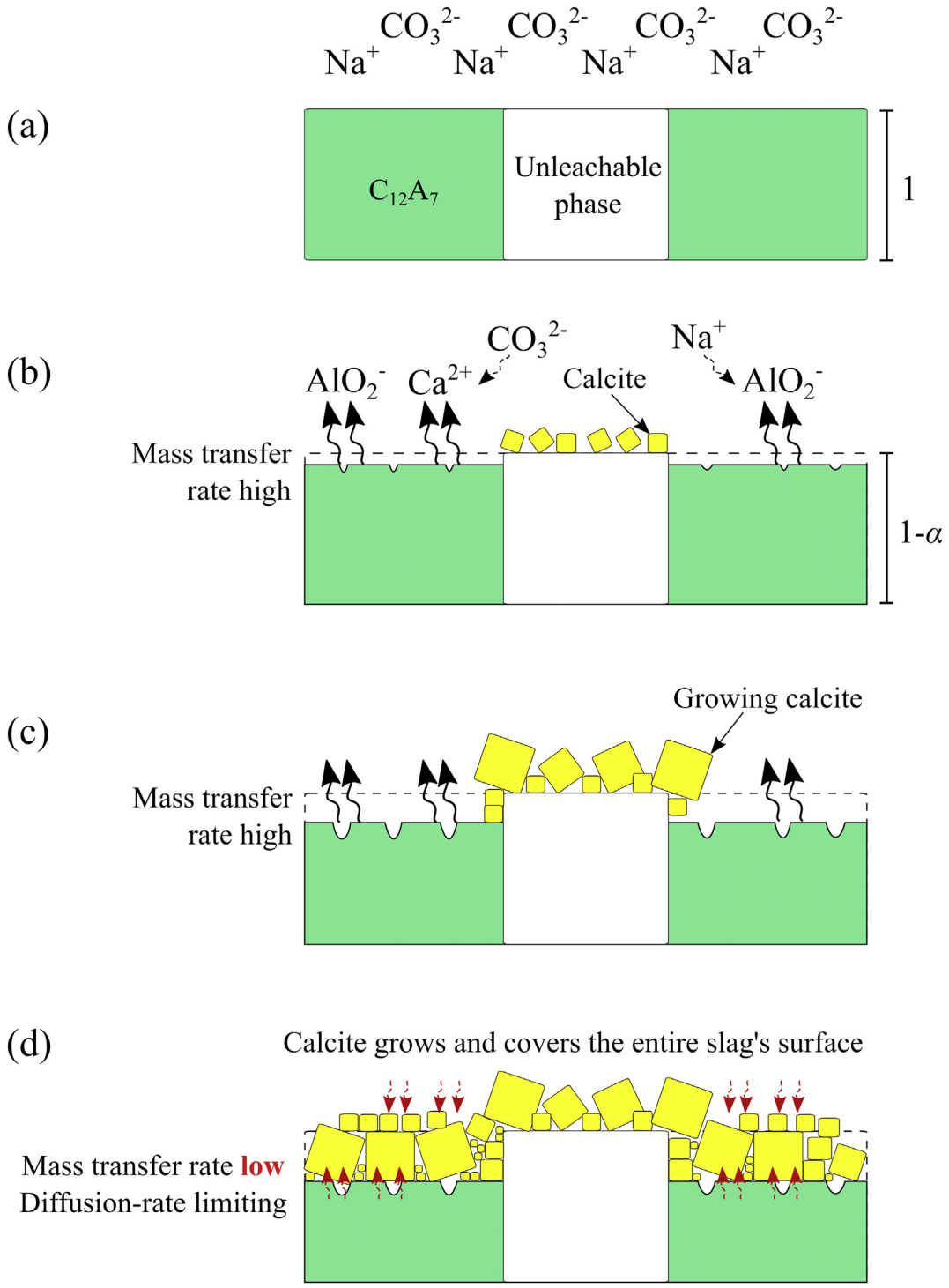

Fig. 13. A cross-section view of calcite formation's mechanism during the leaching of $C_{12}A_7$ in Na_2CO_3 solution.

throughout the whole process, as observed in the present study. At the beginning of the leaching process, the calcite does not nucleate at the reacting surface. Therefore, $k_{diff.react}$ and $k_{diff.prod}$ do not exist. Meanwhile, k_{chem} accelerates relatively fast. However, as the calcite layer appears on the reacting surface, the k_{chem} is decreased, and $k_{diff.react}$ and $k_{diff.prod}$ become progressively more critical. Thus, by eliminating the intermediate concentrations difference between these steps, we can straightforwardly combine the rate constant as an apparent process rate constant ($k_{overall}$) as shown in Eq. (5):

$$\frac{1}{k_{overall}} = \frac{1}{k_{chem}} + \frac{1}{k_{diff.react}} + \frac{1}{k_{diff.prod}} \quad (5)$$

Based on the pH measurement in Fig. 8 and SEM result in Fig. 12, we suggest that the k_{chem} value is obtained as the leaching reaction starts. Moreover, the rate is expected to decrease significantly after 15 min of leaching, as the calcite layers completely cover the slag surface. Subsequently, the reaction is diffusion-controlled as it is mainly dependent on the $k_{diff.react}$ and $k_{diff.prod}$.

The value of $k_{chem}^{-1}$is suggested to be significantly low as the chemical reaction rate is immediate and, therefore, can be neglected. As

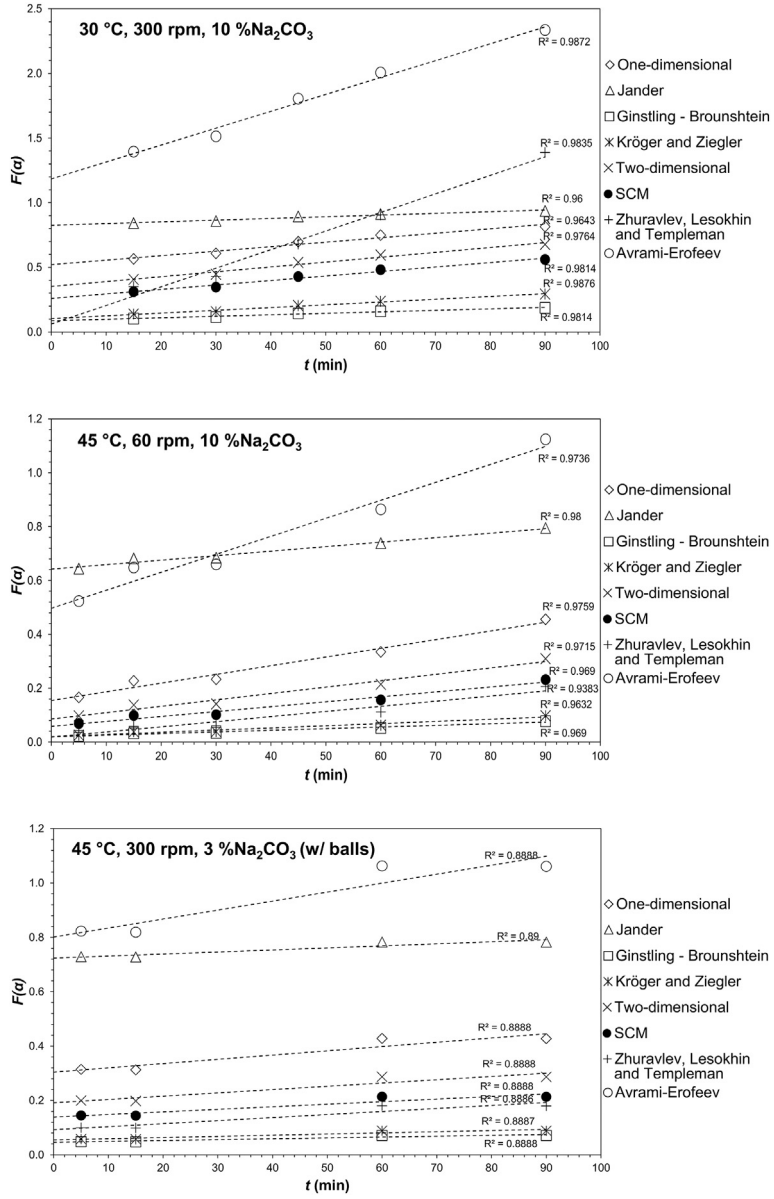

Fig. 14. Different kinetics rate modelling, *F(α)*, as a function of time (min) in different leaching conditions: (a) 30 °C, 300 rpm, 10 wt%Na_2CO_3, (b) 45 °C, 60 rpm, 10 wt%Na_2CO_3, (c) 45 °C, 300 rpm, magnetic bar and PTFE-balls as stirrer, and 3 wt%Na_2CO_3.

Table 4
Apparent process rate constant that corresponds to the leaching conditions.

Leaching conditions (temperature, stirring rate, Na_2CO_3 concentration)	Apparent process rate constant ($k_{overall}$)
45 °C, 300 rpm, 3%	7×10^{-3}
90 °C, 300 rpm, 3%	18×10^{-3}
30 °C, 300 rpm, 10%	10×10^{-3}
45 °C, 300 rpm, 10%	12×10^{-3}
45 °C, 60 rpm, 10%	6×10^{-3}

the diffusion of reactant and product happen at the same time, it is challenging to separate $k_{diff.react}$ and $k_{diff.prod}$ values. We may use the GB-equation to calculate the $k_{overall}$ based on the experimental results in Section 5.2, as shown in Table 4, and suggest that the sum of ${k_{diff.\ react}}^{-1}$and ${k_{diff.\ prod}}^{-1}$is the same as ${k_{overall}}^{-1}$. It is also worth to note that the diffusion rate of Ca^{2+} and AlO_2^- ions (products) eventually can go slower and slower than Na^+ and ${CO_3}^{2-}$ ions (reactants), mainly when the calcite layer builds upon the surface of the slag, which leads to the accumulation of Ca^{2+} and AlO_2^- ions beneath the calcite layers as illustrated previously in Fig. 13(d).

As seen in Table 4, the rate of $k_{overall}$ increases with increasing temperature, stirring rate, and concentration of Na_2CO_3. By increasing the leaching temperature 2 times, we may have up to 2.6 times higher rate, depending on solution concentration. At the same temperature and stirring rate, we may have a 1.7 times higher rate by increasing three times of the Na_2CO_3 concentration. Furthermore, as we observed that the leaching reaction rate is influenced by temperature, the relationship between the apparent process rate constant and temperature can be described using the Arrhenius equation as given in Eq. (6):

$$k_{overall} = A \times \exp\left[\frac{-E}{RT}\right] \tag{6}$$

where A is a pre-exponential factor, E is the apparent activation energy, R is the universal gas constant 8.3145 J/mol·K, and T is the absolute temperature in K. The apparent activation energy can be calculated by plotting the natural logarithm of $k_{overall}$ against 1000/T, as shown in Fig. 15 where the slope represents -*E*/*R* ratio. The results show that the

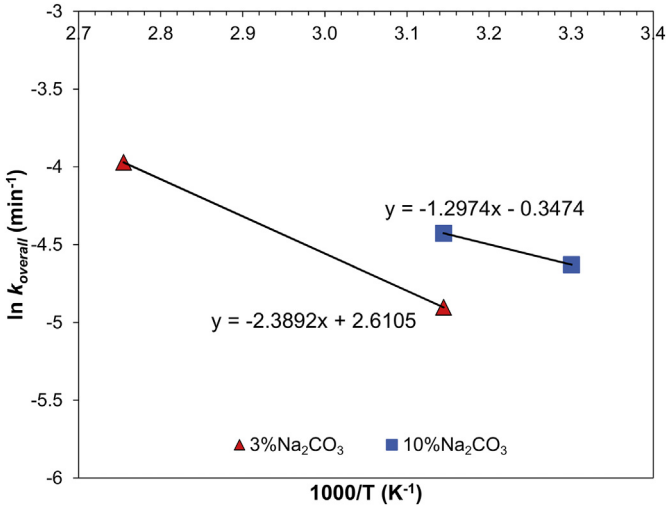

Fig. 15. Arrhenius plot of the slag dissolution at different leaching temperatures and solvent concentrations.

apparent activation energy for the leaching process at 3 wt% and 10 wt % Na_2CO_3 concentrations are 19.9 and 10.8 kJ/mol, respectively. The value of apparent activation energy is relatively low that supports our hypothesis that the reaction is a diffusion rate limiting. The result is in agreement with Tong and Li (Tong and Li, 2017) where they have calculated the apparent activation energy of a leaching reaction between calcium aluminate slag and Na_2CO_3. It is also confirmed by other studies that the apparent activation energy of hydrometallurgical reactions controlled by diffusion is either < 15 kJ/mol (Free, 2013) or < 40 kJ/mol (Jackson, 1986). Moreover, the pre-exponential factor is calculated by using Eq. (6), which is 1.18×10^{-2} /min, on average.

6. Conclusion

A series of leaching treatment of a calcium aluminate slag in Na_2CO_3 solution has been done. The observation on kinetics and leaching mechanism can be summarized as follows:

1. Leaching reactions between leachable phases, e.g., $12CaO{\cdot}7Al_2O_3$, $CaO{\cdot}Al_2O_3$, and Na_2CO_3, are relatively fast. High alumina recovery up to 90.5% is obtained within 90 min after the slag is leached at 10 wt% Na_2CO_3 solution, high stirring rates, at 30–45 °C.
2. The calcite phase as a solid product of the leaching reaction starts to nucleate at the surface of the adjacent non-leachable phase in the slag. Calcite crystals can grow up to large sizes (over 10 μm), and bridging occurs between them (agglomeration tendency).
3. The use of stirrer and PTFE-ball during the leaching (wet-grinding) increases the collision frequency between both slag and stirrer that breaks the calcite layer and the agglomerates that leads to higher alumina recovery.
4. Different kinetic models were tried to find out the rate-limiting step during the leaching, and it was found that the diffusion of reactant and productions controls the process rate through the product calcite layer.
5. The calculated apparent activation energy of the leaching reaction is 10.8–19.9 kJ/mol. The values are relatively low, which indicates the reaction is diffusion rate limited.

Declaration of Competing Interest

The authors declare that they have no known competing financial interests or personal relationships that could have appeared to influence the work reported in this paper.

Acknowledgment

The NTNU has funded the research, and the work was supported by the Research Domain 5 – Materials and the Society in SFI Metal Production (Project no. 237738). The support from the ENSUREAL project (EU Horizon 2020) is also acknowledged.

Appendix A. Supplementary data

Supplementary data to this article can be found online at https://doi.org/10.1016/j.hydromet.2020.105388.

References

Azof, F.I., Kolbeinsen, L., Safarian, J., 2017. The leachability of calcium aluminate phases in slags for the extraction of alumina. In: Travaux 46, Proceedings of 35th International ICSOBA Conference. ICSOBA, Hamburg, pp. 243–253.
Azof, F.I., Kolbeinsen, L., Safarian, J., 2018. Characteristics of calcium-aluminate slags and pig iron produced from smelting-reduction of low-grade bauxites. Metall. Mater. Trans. B Process Metall. Mater. Process. Sci. 49, 2400–2420. https://doi.org/10.1007/s11663-018-1353-1.
Azof, F.I., Kolbeinsen, L., Safarian, J., 2019. Kinetics of the leaching of alumina-containing slag for alumina recovery. In: Proceedings of EMC 2019, pp. 511–526.
Azof, F.I., Vafeias, M., Panias, D., Safarian, J., 2020. The leachability of a ternary CaO-Al2O3-SiO2 slag produced from smelting-reduction of low-grade bauxite for alumina recovery. Hydrometallurgy 191, 105184. https://doi.org/10.1016/j.hydromet.2019.105184.
Blake, H.E., Fursman, O.C., Fugate, A.D., Banning, L.H., 1966. Adaptation of the Pedersen Process to the Ferruginous Bauxites of the Pacific Northwest, Bureau of Mines US Department of the Interior.
Free, M.L., 2013. Hydrometallurgy: Fundamentals and Applications. John Wiley & Sons, Inc, New Jersey.
Fursman, O.C., Blake Jr., H.E., Mauser, J.E., 1968. Recovery of Alumina and Iron from Pacific Northwest Bauxites by the Pedersen Process. Albany.
Ginstling, A.M., Brounshtein, B.L., 1950. Concerning the diffusion kinetics of reactions in spherical particles. Appl. Chem. USSR 23, 1327–1338. https://doi.org/10.1007/10722086_4.
Jackson, E., 1986. Hydrometallurgical Extraction and Reclamation. Ellis Horwood, Chichester.
Khawam, A., Flanagan, D.R., 2006. Solid-state kinetic models: basics and mathematical fundamentals. J. Phys. Chem. B 110, 17315–17328. https://doi.org/10.1021/jp062746a.
Levenspiel, O., 1999. Chemical Reaction Engineering, 3rd ed. John Wiley & Sons, Inc.
McIlvried, H.G., Massoth, F.E., 1973. Effect of particle size distribution on gas-solid reaction kinetics for spherical particles. Ind. Eng. Chem. Fundam. 12, 225–229. https://doi.org/10.1021/i160046a014.
Miller, J., Irgens, A., 1974. Essential Readings in Light Metals, Essential Readings in Light Metals. Springer International Publishing, Cham. https://doi.org/10.1007/978-3-319-48176-0.
Nancollas, G., Reddy, M., 1971. The crystallization of calcium carbonate. II. Calcite growth mechanism. J. Colloid Interface Sci. 37, 824–830. https://doi.org/10.1016/0021-9797(71)90363-8.
Pedersen, H., 1927. Process of Manufacturing Aluminum Hydroxide. pp. 1618105.
Safarian, J., Kolbeinsen, L., 2016a. Sustainability in alumina production from bauxite. In: Sustainable Industrial Processing Summit, pp. 75–82.
Safarian, J., Kolbeinsen, L., 2016b. Smelting-reduction of bauxite for sustainable alumina production. In: Sustainable Industrial Processing Summit, pp. 149–158.
Sellaeg, H., Kolbeinsen, L., Safarian, J., 2017. Iron separation from bauxite through smelting-reduction process. In: Minerals, Metals and Materials Series, pp. 127–135. https://doi.org/10.1007/978-3-319-51541-0_19.
Tong, Z., Li, Y., 2017. Leaching Behavior of Alumina from Smelting Reduction Calcium Aluminate Slag with Sodium Carbonate Solution. pp. 37–43. https://doi.org/10.1007/978-3-319-51541-0.
Tsesmelis, K., 2017. Bauxite mine rehabilitation & bauxite residue management: A global perspective. In: Proceedings of 35th International ICSOBA Conference. ICSOBA, pp. 71.
Vafeias, Michail, Marinos, Danai, Panias, Dimitrios, Safarian, Jafar, Van Der Eijk, Casper, Solhem, Ingeborg, Balomenos, Efthymios, Ksiazek, Michal, Davris, P., 2018. From red to grey: Revisiting the pedersen process to achieve holistic bauxite ore utilisation. In: Proceedings of the 2nd International Bauxite Residue Valorisation and Best Practices Conference, pp. 111–117.
Yagi, S., Kunii, D., 1955. Studies on combustion of carbon particles in flames and fluidized beds. Symp. Combust. 5, 231–244. https://doi.org/10.1016/S0082-0784(55)80033–1.